Development and Validation of a Two-Phase Model for Reinforced Soil by Considering Nonlinear Behavior of Matrix

Ehsan Seyedi Hosseininia, Aff.ASCE[1]; and Orang Farzaneh[2]

Abstract: The paper presents the formulation of a two-phase system applied for reinforced soil media, which accounts for nonlinear behavior of matrix phase. In a two-phase material, the soil and inclusion are treated as two individual continuous media called matrix and reinforcement phases, respectively. The proposed algorithm is aimed to analyze the behavior of reinforced soil structures under operational condition focusing on geosynthetics-reinforced-soil (GRS) walls. The global behavior of such deformable structures is highly dependent to the soil behavior. By accounting for mechanical characteristics of the soil in GRS walls, a relatively simple soil model is introduced. The soil model is formulated in bounding surface plasticity framework. The inclusion is regarded as a tensile two-dimensional element, which owns a linear elastic-perfectly plastic behavior. Perfect bonding between phases is assumed in the algorithm. For validation of the proposed model, the behavior of several single element reinforced soil samples, containing horizontal and inclined inclusions, is simulated and the results are compared with experiment. It is shown that the model is accurately capable of predicting the behavior especially before peak shear strength. The proposed algorithm is then implemented in a numerical code and the behavior of a full-scale reinforced soil wall is simulated. The results of analysis are also reasonably well compared with those of experiment.

DOI: 10.1061/(ASCE)EM.1943-7889.0000111

CE Database subject headings: Constitutive models; Soil stabilization; Geosynthetics; Numerical analysis; Matrix methods.

Author keywords: Constitutive models; Reinforced soil; Geosynthetics; Multiphase material; Numerical analysis.

Introduction

Reinforced soil is a construction material in which the soil is strengthened by reinforcing inclusions such as steel bars or geosynthetic sheets. This technique is actually a mechanical improvement of the soil by such tensile elements through their shear interaction. The reinforced soil mass has been regarded as a composite system like other civil engineering materials (e.g., plain concrete, reinforced concrete, mixed soil, etc.) and has been analyzed by homogenization methods which present its macrobehavior based on microstructure elements (soil and inclusion). That is due to the existence of repeated layers of soil and reinforcing elements in a periodic manner. In this regard, an equilibrium medium is introduced which behaves, at the macroscopic level, as a homogenous but anisotropic composite material. (e.g., Harrison and Gerrard 1972; Romstad et al. 1976; Michalowski and Zhao 1995; de Buhan et al. 1989).

In domain of theories applied for periodic media, de Buhan and Sudret (1999) have recently proposed a new approach which is called "multiphase model." This approach is actually a mechanical framework, based on virtual work method, which explains a macroscopic description of a composite medium as the superposition of individual continuous media called phases. Each point of the geometry in a multiphase material is comprised of matrix phase (representative of the element which covers the most part of space) and reinforcement phases (representative of axial inclusions existing in different directions) with their own kinematics. In a multiphase material, each phase has its own specific behavior for both elastic and plastic regimes including deformational and yield characteristics. Hence, the global behavior of the composite is the outcome of all phases' behavior engaged with each other through strain compatibility. In fact, this framework can be regarded as an extension of a homogenization procedure, in the sense that the composite is represented at the macroscopic scale not by one single medium as in the homogenization procedure, but by several superposed mutually interacting media.

The multiphase model was used for analyzing the media reinforced by one-dimensional elements (such as bolt, pile, etc.) which only supported axial compression-tension forces. The medium was hence considered as a two-phase material. The examples are numerical studies of a piled-raft group (de Buhan and Sudret 2000) and a rock-bolted tunnel (Sudret and de Buhan 2001). The model was then developed in order that the flexural (de Buhan and Sudret 2000) and shear behavior (Hassen and de Buhan 2005) of such linear inclusions were taken into consideration. All the analyses were performed with the hypothesis of perfect bonding between phases. Although the same strain compatibility exists in traditional homogenization methods, the advantage of the multiphase approach is the ability to manifest the hardening behavior of the reinforced mass due to incompatibility among plastic strains of each phase (Sudret 1999). Later on, relative displacement between phases was considered in the formulation in a simplified manner (Bennis and de Buhan 2003; de Buhan et al. 2008). More recently, Thai et al. (2009) have numerically studied the stability of a retaining wall in which the backfill was

[1]School of Civil Engineering, University College of Engineering, Univ. of Tehran, Shanzdah Azar Ave., Enghelab St., P.O. Box 14155–6457, Tehran, Iran (corresponding author). E-mail: eseyedi@ut.ac.ir

[2]School of Civil Engineering, Faculty of Engineering, Univ. of Tehran, Tehran, Iran. E-mail: ofarzane@ut.ac.ir

Note. This manuscript was submitted on July 29, 2008; approved on November 11, 2009; published online on November 4, 2009. Discussion period open until November 1, 2010; separate discussions must be submitted for individual papers. This paper is part of the ***Journal of Engineering Mechanics***, Vol. 136, No. 6, June 1, 2010. ©ASCE, ISSN 0733-9399/2010/6-721–735/$25.00.

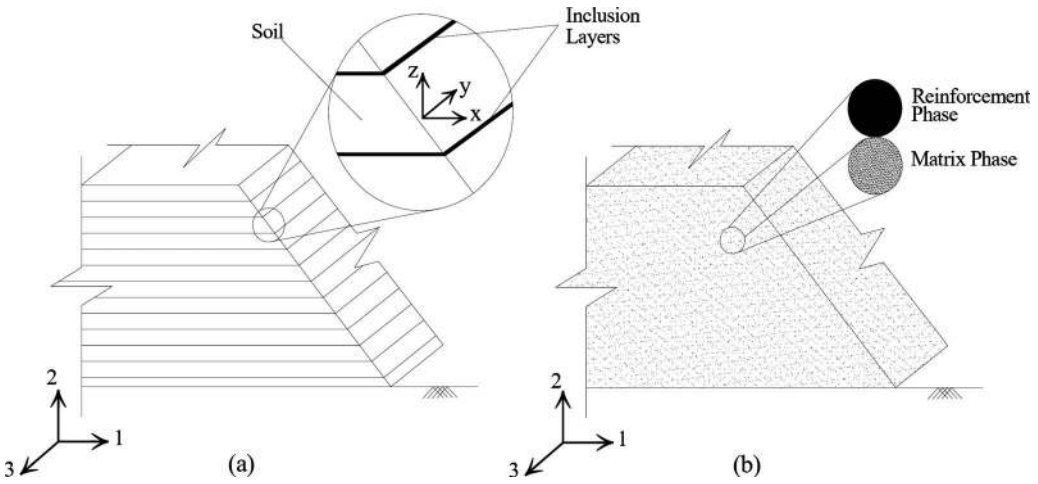

Fig. 1. Presentation of a reinforced soil in different scales of view: (a) microscopic scale in which both soil and inclusion can be recognized in the structure; (b) Macroscopic scale where each geometrical point includes both matrix and reinforcement phases. The medium is considered as two-phase system.

reinforced by strips. The deformational behavior of the structure was not studied; however, by accounting for failure mechanisms generated in the reinforced soil mass, the results have been evaluated by those of upper bound limit analysis. It is mentioned that in all the analyses mentioned above, the behavior of both soil and inclusions was taken as linear elastic—perfectly plastic.

Apart from the stability of reinforced soil walls which is the subject of conventional design (limit state) methods, the deformational behavior of such structures is an important issue to evaluate their performance. This topic is more highlighted for geosynthetic-reinforced soil (GRS) walls in comparison with the walls reinforced by metallic strips. This is due to the extensibility of geosynthetic inclusions, which influences the overall load-deformation behavior of soil-inclusion systems (McGown et al. 1978). As a result, deformational behavior of such flexible composite is highly dependent to the soil behavior. In other words, the most important issue in design of GRS walls is the deformation pattern during its serviceability. Karpurapu and Bathurst (1995) demonstrated that correct modeling of the dilatant behavior of soil is required to give accurate predictions of reinforced wall performance. Holtz and Lee (2002) indicated that considering confining pressure in the soil behavior is an important issue in accurately predicting the wall face deformation. Hence, simple soil models such as linear elastic-perfectly plastic models would not be suitable for simulating the GRS medium behavior and applying a more rigorous soil constitutive model should be considered as a priority (e.g., Helwany et al. 1999; Desai and El-Hoseiny 2005; Ling et al. 2000).

On the other hand, when the GRS wall is under service (working stress) condition, it might be said that relative displacement between soil and inclusion is of less importance. In fact, most of numerical studies reported in the literature have used perfect bonding between the soil and inclusion (e.g., Leshchinsky and Vulova 2001; Ling and Leshchinsky 2003). Hatami and Bathurst (2005, 2006) have constructed, instrumented and monitored several full-scale GRS walls. The walls were then loaded up to service surcharge. They have reported that no relative displacement between the reinforcing layers and the soil was observed. They obtained a good agreement between numerical simulations and measured data by supposing a full rigid contact between reinforcement layers and the soil. Other researchers have performed the same approach in numerical analyzes of reinforced soil structures and results have been confirmed by comparing them with experimental data (e.g., Ling et al. 2000; Holtz and Lee 2002; Guler et al. 2007). This approach in discrete modeling of reinforced soil systems justifies that considering perfect bonding in a two-phase system is acceptable when the analysis is aimed to study the structure behavior under operational condition.

As a main objective of the present paper, we develop the formulation of the two-phase material by applying a nonlinear elastoplastic soil model under monotonic loading path. In the present contribution, we focus on the numerical simulations that can be used to predict the operational condition of reinforced soil systems rather than initiation of collapse. A model for noncohesive granular soils is introduced within the framework of bounding surface plasticity. The inclusion is considered as a tensile planar element (such as geotextile and geogrid layers), which behaves as a linear elastic-perfectly plastic material. The governing constitutive equations of each element are introduced separately and then they are used as those of their corresponding phases within the multiphase concept. Perfect bonding is assumed between phases. We evaluate the presented model by simulating the behavior of several single element reinforced sand samples in which the inclusions are placed in horizontal as well as inclined directions. In order to solve boundary value problems, the proposed algorithm is implemented in a numerical code and the behavior of a full-scale reinforced soil wall is studied.

Description of Reinforced Soil as a Two-Phase System

Consider a reinforced soil mass in the global coordinate system 1-2-3, in accordance with Fig. 1(a), in which the planar inclusions with thickness t are placed in a periodic manner with the same spacing h from each other. We take a local coordinate system x-y-z for the inclusion. The y-axis of the inclusion is always considered to be parallel to the 3-axis of the global coordinate system. As a general case, the inclusion direction may have an angle of α with horizontal (the 1-3 plane). Such a medium can be replaced by a two-phase material, as shown in Fig. 1(b), which is consisted of two continuous media (or phases) having mutual

interaction. From view of macroscopic scale, each geometrical point of such two-phase material is decomposed into matrix phase (labeled as m), on the one hand, which represents the soil and reinforcement phase (labeled as r), on the other hand, which is the macroscopic counterpart of inclusion network.

The statics equations derived from the kinematics of each phase may be obtained by means of the virtual work method (Sudret 1999; de Buhan and Sudret 2000). The equilibrium equations for each phase can be written separately as follows:

$$div\sigma_{ij}^{m} + \rho^{m}F_{i}^{m} + I_{i} = 0 \tag{1}$$

for the matrix phase, and

$$div\sigma_{ij}^{r} + \rho^{r}F_{i}^{r} - I_{i} = 0 \tag{2}$$

for the reinforcement phase. σ_{ij}^{m} (resp. σ_{ij}^{r}) denotes the classical Cauchy stress tensor defined in every point of the matrix (resp. reinforcement) phase. The term $\rho^{m}F_{i}^{m}$ (resp. $\rho^{r}F_{i}^{r}$) indicates the body force of the matrix (resp. reinforcement) phase. Finally, $+I_i$ (resp. $-I_i$) is the interaction body force exerted by the reinforcement (resp. matrix) phase on the matrix (resp. reinforcement) phase. These equilibrium equations will be completed by the corresponding stress boundary conditions that are prescribed on the boundary surface of each phase separately.

By summing up Eqs. (1) and (2), the global equilibrium equation for a two-phase material appears

$$\text{div}\ \Sigma_{ij} + \rho F_{i} = 0 \tag{3}$$

where

$$\Sigma_{ij} = \sigma_{ij}^{m} + \sigma_{ij}^{r}, \quad \rho F_{i} = \rho^{m}F_{i}^{m} + \rho^{r}F_{i}^{r} \tag{4}$$

Σ_{ij} represents the global stress tensor with partial stresses of all phases. The term ρF_i indicates the body force exerted to the whole mass of the two-phase material.

For each phase, the stress-strain relationship is introduced separately:

$$\sigma_{ij}^{m} = A_{ijkl}^{m}\varepsilon_{kl}^{m}, \quad \sigma_{ij}^{r} = A_{ijkl}^{r}\varepsilon_{kl}^{r} \tag{5}$$

where A_{ijkl}^{m} (resp. A_{ijkl}^{r}) indicates the stiffness tensor of the matrix (resp. reinforcement) phase. Besides, the evolution of stress state in each phase is governed by its corresponding yield criterion which defines the onset of plastic (irreversible) deformation in the phase.

In general case, the phases may have kinematics different from each other, resulting in different strain fields ε_{ij}^{m} and ε_{ij}^{r} for matrix and reinforcement phases, respectively. The interaction body force (I_i) in Eqs. (1) and (2) can be defined as a function of relative displacement between phases. In the case of perfect bonding, the displacement field of matrix and reinforcement phases becomes identical. This makes the analysis less sophisticated since there would be no need to calculate the displacement of the phases in each geometrical point. In this case, we have

$$\in_{ij} = \varepsilon_{ij}^{m} = \varepsilon_{ij}^{r} \tag{6}$$

in which $\in_{ij}$ denotes the strain tensor of the two-phase material. By considering such strain compatibility condition, the global stress-strain relationship can be obtained by summing up partial stress tensors

$$\Sigma_{ij} = (A_{ijkl}^{m} + A_{ijkl}^{r}) \in_{kl} \tag{7}$$

Inclusion Behavior

As mentioned before, the inclusion is considered as a planar form. The behavior of the inclusion is described in the local coordinate system x-y-z. The thickness in z direction is so small as to be negligible in comparison with other dimensions in its plane. It is assumed that the inclusion has an isotropic linear elastic-perfectly plastic behavior with Young modulus (E^{inc}), Poisson's ratio (υ^{inc}), and yield stress ($\sigma_{\text{yield}}^{\text{inc}}$). Moreover, the inclusion only supports tensile stresses whose sign is considered as negative. No shear stress can be exerted in the x-y plane of the inclusion. The incremental stress-strain relationship for a bidimensional element has the following form according to the elasticity theory:

$$\begin{Bmatrix} \dot{\sigma}_{x}^{\text{inc}} \\ \dot{\sigma}_{y}^{\text{inc}} \end{Bmatrix} = \frac{E^{\text{inc}}}{(1-\nu^{\text{inc}2})} \begin{bmatrix} 1 & \nu^{\text{inc}} \\ \nu^{\text{inc}} & 1 \end{bmatrix} \begin{Bmatrix} \dot{\varepsilon}_{x}^{\text{inc}} \\ \dot{\varepsilon}_{y}^{\text{inc}} \end{Bmatrix} \tag{8}$$

where σ_x and σ_y=in-plane stresses and ε_x and ε_y are corresponding strains. The over dot denotes the incremental form of the parameters. The yield function of the inclusion (f^{inc}) in a two-dimensional space is in the form of Tresca criterion

$$f^{\text{inc}}(\sigma_{x}^{\text{inc}}, \sigma_{y}^{\text{inc}}) = |\sigma_{x}^{\text{inc}} - \sigma_{y}^{\text{inc}}| \leqslant |\sigma_{\text{yield}}^{\text{inc}}| \tag{9}$$

Under the condition of plane strain (in the 1-2 plane), such as what exists in the most reinforced soil wall analysis cases, deformation in y-direction is considered to be zero. Hence, Eqs. (8) and (9) for such planar inclusion turns into one-dimensional form as follows:

$$\dot{\varepsilon}_{x}^{\text{inc}} = 0 \Rightarrow \dot{\sigma}_{y}^{\text{inc}} = \nu^{\text{inc}}\dot{\sigma}_{x}^{\text{inc}}, \quad \dot{\sigma}_{x}^{\text{inc}} = \left[\frac{E^{\text{inc}}}{1-\nu^{\text{inc}2}}\right]\dot{\varepsilon}_{x}^{\text{inc}} \tag{10}$$

$$f^{\text{inc}}(\sigma_{x}^{\text{inc}}) = |\sigma_{x}^{\text{inc}}| \leqslant \left|\frac{\sigma_{\text{yield}}^{\text{inc}}}{(1-\nu^{\text{inc}2})}\right| \tag{11}$$

In order to define macroscopic properties of the reinforcement phase in terms of those of the inclusion, the reinforcement volume fraction (χ), which is usually very small, is introduced as the ratio of the inclusion volume (V^{inc}) to that of the soil (V^{s})

$$\chi = \frac{V^{\text{inc}}}{V^{s}} = \frac{t}{h} \tag{12}$$

The generalized stress tensor in the reinforcement phase, which corresponds to the in-plane stresses, appears in the following form:

$$\sigma_{ij}^{r} = \sigma_{x}^{r}(e_{i}^{r} \otimes e_{j}^{r}) + e_{y}^{r}(e_{i}^{3} \otimes e_{j}^{3}) \tag{13}$$

in which $\sigma_{i}^{r} = \chi\sigma_{i}^{\text{inc}} (i = x, y)$. The vectors $\{e^{r}\} = \{\cos\alpha, \sin\alpha, 0\}$ and $\{e^{3}\} = \{0, 0, 1\}$ indicate the direction of reinforcement phase in 1-2 plane and the 3-axis, respectively. In the equation above, the symbol $\otimes$ indicates dyadic product of vectors. Also, the mechanical properties (without any change in Poisson's ratio) are defined as follows:

$$E^{r} = \chi E^{\text{inc}}, \quad \sigma_{\text{yield}}^{r} = \chi\sigma_{\text{yield}}^{\text{inc}} \tag{14}$$

Finally, the global stiffness tensor of the reinforcement phase (A_{ijkl}) is defined in the following form:

$$A_{ijkl} = E^{r}(e_{i}^{r} \otimes e_{j}^{r} \otimes e_{k}^{r} \otimes e_{l}^{r}) \tag{15}$$

Calculation of Parameters

By applying a uniaxial extension test along x-direction on a reinforcing sheet with a defined width and length, Young modulus can be determined from average slope of load-elongation curve, J_{ave}, expressed in units of force per unit length, divided by thickness (t). It means: $E^{inc}=J_{ave}/t$. Poisson's ratio is usually introduced by the manufacturer. Finally, since the lateral stress (σ_y^{inc}) in an extension test of the sheet is zero, the yield stress (σ_{yield}^{inc}) equals the yield applied force per unit length (T^{yield}) divided by thickness, i.e., $\sigma_{yield}^{inc}=T^{yield}/t$. Procedures for measuring tensile properties of geotextile can be found in the standard test ASTM D4595-09 (ASTM 2009).

Soil Behavior

In the literature review of soil modeling, one can encounter a number of soil constitutive models regarding elastic and plastic behaviors for different loading paths. A comprehensive comparison among different soil models can be found in Seyedi Hosseininia (2008). In the present research, we introduce a simple constitutive model for noncohesive granular soils in such a way that: (1) the soil behavior is simulated as well as possible with the least number of model parameters for monotonic loading paths; (2) the parameters can be easily measured in a straightforward manner from traditional tests; (3) the formulation can be improved properly for future extensions in order to consider different aspects of soil behavior (such as critical state, anisotropy, etc.) and loading conditions (such as cyclic response). To these aims, the soil constitutive model is introduced within the bounding surface plasticity framework (Dafalias and Popov 1975; Krieg 1975) whose ability has already been proven to properly predict stress-strain relationships of geomaterials (e.g., Yang et al. 1985; Wang et al. 1990; Li 2002). According to this framework, a yield surface always places inside the other surface called as bounding surface. The magnitude of plastic strain increment is defined as a direct function of distance between current stress state on yield surface from a conjugate (image) stress state defined on the bounding surface. The proposed model is based on the following main assumptions:

1. The model parameters are not dependent to the void ratio. In other words, a set of parameters are presented for a specific degree of density. This assumption is justifiable since reinforced soil structures (such as GRS walls) are constructed in such a way that the granular soil layers are placed according to a controlled procedure with a nearly constant density;
2. The model cannot predict post peak softening behavior. In the literature review of GRS walls behavior analysis, the soil models used are mostly chosen in such a way that they only takes into consideration the behavior of soil up to the peak soil strength (e.g., Guler et al. 2007; Hatami and Bathurst 2005, 2006; Helwany et al. 1999; Holtz and Lee 2002; Ling et al. 2004). It is also worth mentioning that Bathurst et al. (2005) have investigated separately the behavior of a full-scale GRS wall under working stress condition as well as that of soil samples alone and have indicated that different parts of the wall experienced strain levels less than or around the soil peak strength shear strains. In these strain levels, contiguous failure zones do not generate in the reinforced soil zone and thus, the soil does not reach its ultimate (limit) state. In addition, Allen et al. (2003) have expressed that the soil would not attain its post peak behavior within the structures under working stress condition where the strain level in the reinforced soil mass is smaller than a limited value; and
3. The peak strength of the soil (ϕ_{peak}) is assumed constant. The same assumption is considered for the parameter ϕ_{PTL}, as explained later, which describes dilative/contractive behavior of the soil. It is examined that the value of these parameters changes slightly in the range of applied stress levels in reinforced soil structures and the error resulting from this assumption is ignorable in predicting the behavior (Pastor et al. 1990; Manzari 1994; Seyedi Hosseininia 2008).

All stresses are considered as effective since the medium is under drained condition. The stress and strain components are considered as positive in compression and negative in tension. The formulation is presented in terms of principal stress and strain components. This results in a simple and comprehensive form of equations so that it can be easily implemented in a numerical code.

The total strain increment is supposed to be composed of two parts: elastic and plastic. That is

$$\dot{\varepsilon}_i = \dot{\varepsilon}_i^e + \dot{\varepsilon}_i^p \tag{16}$$

where ε_i represents the strain component correspondent to principal stress direction. Dot sign indicates incremental form of the corresponding parameter. The superscripts e and p stand for the elastic and plastic parts of the total strain increment, respectively. In the following subsections, elastic and plastic behavior parts are derived and by summing them up, the global stress-strain relationship of the constitutive equation will be introduced.

Elastic Behavior

Incremental elastic strain portion is obtained from the generalized Hooke's law in terms of shear modulus (G) and Poisson's ratio (υ)

$$\dot{\varepsilon}_i^e = \frac{1}{2G(1+\nu)}\left[\dot{\sigma}_i - \nu\sum_{j\neq i}\dot{\sigma}_j\right] \tag{17}$$

It is assumed that the Poisson's ratio is constant in the model. According to empirical studies based on the measurement of elastic shear modulus of granular media (e.g., Duncan and Chang 1970), a nonlinear relationship as a function of mean effective stress (p) is considered for G

$$G = G_0\left(\frac{P}{P_r}\right)^n \tag{18}$$

G_0 and n are positive model parameters and p_r is a reference pressure (which is considered as the atmospheric pressure =101 kPa). The procedure how to determine these parameters are explained in the calibration section.

Plastic Behavior

The yield surface (f) is expressed in the same form of Mohr-Coulomb surface as a wedge-type shape

$$f(\sigma_1,\sigma_3) = (\sigma_1-\sigma_3) - \sin\varphi_{mob}(\sigma_1+\sigma_3) = 0 \tag{19}$$

where ϕ_{mob}=mobilized friction angle and it is representative of the size of yield surface. σ_1 and σ_3 are major and minor principal stresses, respectively. The intermediate principal stress σ_2 does not play any role in the plastic behavior ($\sigma_3<\sigma_2<\sigma_1$). A similar surface is considered as bounding surface (F^b), where the mobilized friction angle of sand reaches the peak value (ϕ_{peak})

$$F^b(\bar{\sigma}_1,\bar{\sigma}_3) = (\bar{\sigma}_1 - \bar{\sigma}_3) - \sin\varphi_{peak}(\bar{\sigma}_1 + \bar{\sigma}_3) = 0 \quad (20)$$

The bar symbol in the above equation indicates the stress state on the conjugate (image) point over the bounding surface which can be defined by the mapping rule: the conjugate point corresponding to the current stress point is located on the bounding surface with the same effective mean stress (Li and Dafalias 2000).

In the theory of soil plasticity, the coupling between volumetric and shear plastic strain increments can be appropriately described by dilatancy, D, which explains contractive or dilative behavior of sand

$$D = -\dot{\varepsilon}_v^p/\dot{\varepsilon}_q^p \quad (21)$$

where $\dot{\varepsilon}_v^p = \dot{\varepsilon}_1^p + \dot{\varepsilon}_3^p$ and $\dot{\varepsilon}_q^p = \dot{\varepsilon}_1^p - \dot{\varepsilon}_3^p$ represent plastic volumetric and plastic shear (deviatoric) strain increments, respectively. The dilatancy function (D) is introduced as follows:

$$D = D_0[\sin\varphi_{mob} - \sin\varphi_{PTL}] \quad (22)$$

where D_0 is a positive model parameter. ϕ_{PTL} is the mobilized friction angle at which the sand behavior is transformed from being contractive to dilative (e.g., Ishihara 1996). If the sand has loose state, this parameter will get a value close to ϕ_{peak}. Eq. (22) can be regarded as the similar form of the equation introduced, for example, by Nova and Wood (1979), Wang et al. (1990), and Manzari (1994). In the calibration section that follows, it is shown that the model can well predict the soil behavior in both dense and loose states by using this simplification.

Plastic strain increment is calculated according to the nonassociated flow rule

$$\dot{\varepsilon}_i^p = \langle\lambda\rangle\frac{\partial g}{\partial\sigma_i} \quad (23)$$

where g represents plastic potential function of sand and λ is plastic loading index. The McCauley brackets $\langle\ \rangle$ indicate $\langle x\rangle = x$ if $x > 0$ and $\langle x\rangle = 0$, otherwise. Instead of explicitly introducing g function, we herein introduce its derivatives such as what has been done in generalized plasticity (e.g., Mroz and Zienkiewicz 1984; Pastor et al. 1990; Ling and Yang 2006). To this aim, we rewrite Eq. (23) in shear and volumetric form

$$\dot{\varepsilon}_q^p = \langle\lambda\rangle\,\partial g/\partial q, \quad \dot{\varepsilon}_v^p = \langle\lambda\rangle\,\partial g/\partial q \quad (24)$$

in which $q = \sigma_1 - \sigma_3$ is shear stress. Since the normality condition exists in the octahedral (shear) plane of principal stresses (Lade and Duncan 1973), we have: $\partial g/\partial q = \partial f/\partial q$. Hence, by having the derivative of yield function (f) in terms of shear stress (q), i.e., $\partial f/\partial q = 1$ as well as using Eq. (21), one can find: $\dot{\varepsilon}_q^p = \langle\lambda\rangle$ and $\dot{\varepsilon}_v^p = -\langle\lambda\rangle D$. Consequently, the plastic principal strain increments can be calculated

$$\dot{\varepsilon}_1^p = \frac{\langle\lambda\rangle}{2}(1 - D), \quad \dot{\varepsilon}_3^p = \frac{\langle\lambda\rangle}{2}(1 + D) \quad (25)$$

It is reminded that the dilatancy function (D) is a function of stress level in accordance with Eq. (22). At the beginning of loading, the mobilized friction angle (ϕ_{mob}) is smaller than ϕ_{PTL} ($D < 0$), which represents the soil contractive behavior. The growth in ϕ_{mob} initiates the dilative behavior ($D > 0$) by passing through the turning point where D becomes zero at $\phi_{mob} = \phi_{PTL}$. It is worth noting that Eq. (25) is comparable with the incremental plastic strain forms in Mohr-Coulomb model, in which $D = \sin\psi$. The parameter ψ is known as dilatancy angle and it is assumed to be constant. As a consequence, it can be said that the present model accounts for the plastic deformational behavior more precisely than the Mohr-Coulomb model.

Finally, according to the definition of plastic loading index (λ) by the theory of plasticity (Dafalias 1986a), we have

$$\lambda = \frac{1}{K_p}\left(\frac{\partial f}{\partial\sigma_i}\dot{\sigma}_i\right) = \frac{1}{K_p}[(1 - \sin\varphi_{mob})\dot{\sigma}_1(1 + \sin\varphi_{mob})\dot{\sigma}_3] \quad (26)$$

K_p is the plastic modulus and is defined as follows (Dafalias 1986b):

$$K_p = h_0 G\left(\frac{\sin\varphi_{peak} - \sin\varphi_{mob}}{\sin\varphi_{mob}}\right) \quad (27)$$

where h_0 = model parameter. As obvious from the above equation, the plastic modulus is infinite ($K_p = \infty$) at the very beginning of virgin loading, while its value gets close to $K_p = 0$ as far as the mobilized friction angle reaches the bounding limit value ($\varphi_{mob} = \varphi_{peak}$).

General Formulation

Referring back to Eq. (16) and combining elastic [Eq. (17)] and plastic [Eq. (25)] parts of strain increments, the general stress-strain relationship can be established, with some mathematical manipulations, in the following form:

$$\begin{Bmatrix}\dot{\varepsilon}_1\\ \dot{\varepsilon}_2\\ \dot{\varepsilon}_3\end{Bmatrix} = \frac{1}{2G(1+\nu)K_p}\begin{bmatrix} K_p + (1-D)(1-\sin\varphi_{mob})G & -\nu K_p & -\nu K_p - (1-D)(1+\sin\varphi_{mob})G \\ -\nu K_p & K_p & -\nu K_p \\ -\nu K_p - (1+D)(1-\sin\varphi_{mob})G & -\nu K_p & K_p + (1+D)(1+\sin\varphi_{mob})G \end{bmatrix}\begin{Bmatrix}\dot{\sigma}_1\\ \dot{\sigma}_2\\ \dot{\sigma}_3\end{Bmatrix} \quad (28)$$

There are totally six model parameters including ν, G_0, n, D_0, ϕ_{PTL}, and h_0. In the following subsection, we explain how to calibrate their values from conventional tests.

Calibration of Model Parameters

By performing either drained plane strain compression (PSC) or triaxial compression (TC) tests, in which the soil sample is under major (applied stress) and minor (constant lateral stress) principal stresses, all soil model parameters can be easily measured based on curves of deviatoric stress (q) and volumetric strain $\varepsilon_v (= \varepsilon_1 + \varepsilon_2 + \varepsilon_3)$ versus shear strain $\varepsilon_q (= \varepsilon_1 - \varepsilon_3)$. The proposed procedure for calculation of each parameter is shown schematically in Fig. 2 and is explained in detail in sequel.

Poisson's ratio (ν)

Since Poisson's ratio is a parameter in domain of elasticity, it would be difficult to quantify it for soil because the elastic behavior of soils occurs in very small strain range. However, we suppose that the plastic portion of soil behavior is ignorable at the very beginning of loading. Hence, the value of Poisson's ratio is estimated from the initial slope (D_1) of volumetric strain-shear

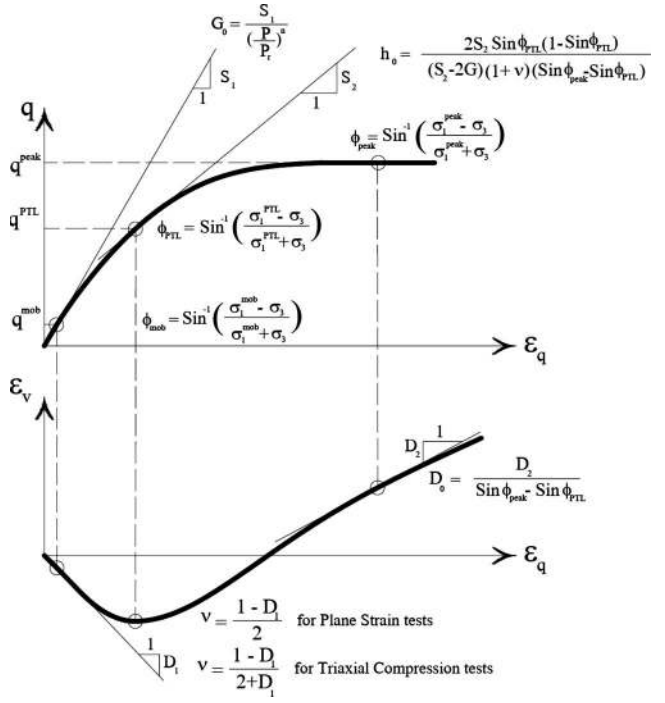

Fig. 2. Calibration method of parameters involved in the soil model based on curves of deviatoric stress and volumetric strain versus shear strain

strain curve at $\varepsilon_q=0$. Regarding different boundary effects in PSC and TC tests, the Poisson's ratio equals (see Appendix)

$$\nu = \frac{1-D_1}{2+D_1} \quad \text{for triaxial test} \tag{29}$$

$$\nu = \frac{1-D_1}{2} \quad \text{for plane strain test} \tag{30}$$

Shear Modulus Coefficients (n and G_0)

If at least three tests with different mean stresses (p) are conducted on same sand samples, these two parameters can be determined by measuring the initial slope of deviatoric stress-shear strain curves as S_1 which is equal to corresponding elastic shear modulus. Referring to Eq. (18) and using Napierian logarithm function [ln (x)] for both sides, it can be rewritten as follows:

$$\ln S_1 = \ln G_0 + n\ln\left(\frac{p}{p_r}\right) \tag{31}$$

Thus, by trending the best straight line through $\ln S_1$ and $\ln (p/p_r)$, both parameters are obtainable. Alternatively, in the absence of data, the value $n=0.5$ is generally acceptable for prediction of sand behavior (e.g., Pastor et al. 1990; Li 2002). Then, G_0 can be assessed by back calculating from S_1.

Determination of ϕ_{peak} and ϕ_{PTL}

Based on Eq. (19), the mobilized friction angle of soil in every arbitrary stress state is assessed by

$$\varphi_{mob} = \sin^{-1}\left(\frac{\sigma_1-\sigma_3}{\sigma_1+\sigma_3}\right) \tag{32}$$

Then, by referring to the deviatoric stress and volumetric strain curves, it is possible to find ϕ_{peak}, where the maximum value of q is reached and ϕ_{PTL}, where the volumetric strain has changed his trace from having a contractive behavior to being dilative.

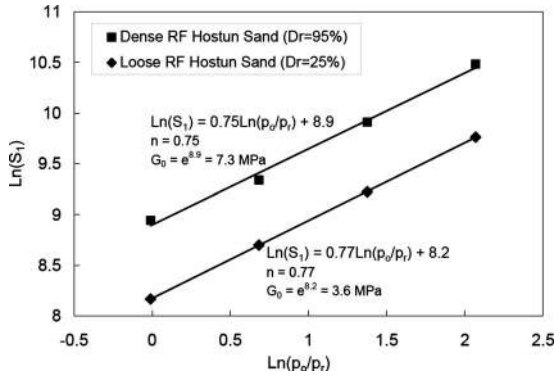

Fig. 3. Determination of elastic shear modulus parameters (G_0 and n) for dense and loose RF Hostun sand

Dilatancy Parameter (D_0)

Having found ϕ_{PTL}, it is possible to assess the value of D_0 from the slope (D_2) of volumetric-deviatoric strain curve in strain levels corresponding to around maximum shear strength ($\phi_{mob}=\phi_{peak}$). According to Eq. (22), we have

$$D_0 = \frac{D_2}{(\sin\varphi_{peak} - \sin\varphi_{PTL})} \tag{33}$$

Hardening Modulus Parameter (h_0)

Based on Eq. (28), the incremental relationship between shear stress and shear strain, by considering $\sigma_3=cte$, can be assessed as follows:

$$\dot{q} = \frac{2G(1+\nu)K_p}{(1+\nu)K_p - 2G(1-\sin\varphi_{mob})}\dot{\varepsilon}_q \tag{34}$$

The fraction in the right hand side in the above equation indicates tangential slope of an arbitrary point in the deviatoric stress-strain curve. As a consequence, the parameter h_0 is calculated by having the tangential slope (S_2) at any point. Considering the tangential slope at the ϕ_{PTL} point, for example, we obtain

$$h_0 = \frac{2S_2(1-\sin\varphi_{mob})\sin\varphi_{mob}}{(1+\nu)(\sin\varphi_{peak} - \sin\varphi_{mob})(S_2-2G)} \tag{35}$$

Evaluation of Soil Model

In order to show the ability of the proposed sand model, we herein simulate the behavior of sand in plane strain condition. Besides, the soil behavior under triaxial condition will be simulated and the results will be presented in the upcoming section where the behavior of a reinforced soil wall is studied.

Desrues and Viggiani (2004) have carried out a series of PSC tests on dense ($D_r=95\%$) and loose ($D_r=25\%$) RF Hostun sand under drained condition and different lateral pressures of 100, 200, 400, and 800 kPa. We have assessed all the model parameters based on the procedure mentioned in the calibration section. Fig. 3 shows the relationship between $\ln(S_1)$ and $\ln(p_o/p_r)$ from which the parameters G_0 and n are obtained. In each curve, the other parameters (such as ϕ_{peak} and ϕ_{PTL}) have been obtained which are found to be almost in the same order. The mean values of all sand parameters are reported in Tables 1 and 2 for dense

Table 1. Model Parameters of Dense RF Hostun Sand (D_r=95%)

v (-)	G_0 (MPa)	n (-)	D_0 (-)	ϕ_{PTL} (deg)	h_0 (-)	ϕ_{peak} (deg)
0.40	7.30	0.75	1.04	30.7	0.40	45.20

and loose RF Hostun sand samples, respectively. As can be seen, the ϕ_{peak} value for the dense group is obtained higher than loose group, which is reasonable. Moreover, since the loose samples tend to dilate hardly in large strains, it can be seen that the ϕ_{PTL} value is assessed close to ϕ_{peak}, while this is not the case in dense group and the transition from contractive to dilative behavior takes places in small stress levels.

The results of experimental tests as well as the simulation of sand behavior by the proposed formulation are demonstrated together in Fig. 4 for dense and loose samples. As can be seen, there is a good agreement between experimental and simulation results in stress and strain spaces for a large range of stresses (100–800 kPa), especially for dense sand which is the most case existing in a reinforced soil medium.

Table 2. Model Parameters of Loose RF Hostun Sand (D_r=25%)

v (-)	G_0 (MPa)	n (-)	D_0 (-)	ϕ_{PTL} (deg)	h_0 (-)	ϕ_{peak} (deg)
0.40	3.60	0.77	0.80	31.80	1.48	33.30

Numerical Implementation

The proposed formulation is implemented in the finite difference-based code FLAC (Itasca Consulting Group 2001). Since two types of material (matrix and reinforcement phases) exist in each element, stress-strain calculation is performed separately for each phase. It is first assumed that applied total strain increment on the two-phase system is elastic. Therefore, elastic trial stresses in both phases are calculated. Then, it is examined if the stresses violate yield criteria. If the stress state lies outside its yield function, stress state is corrected by plastic correction procedure used in FLAC (explicit procedure). The calculation is initially launched for the matrix phase. The calculation then continues for the reinforcement phase. Having found stress levels in both phases, the global stress tensor in the mass is calculated by summing up the partial stresses of two phases [Eq. (4)].

Simulation of Reinforced Soil as a Two-Phase System

In order to validate the proposed constitutive model by the two-phase formulation, in this section, the behavior of several reinforced soil samples is simulated which are loaded in a PSC apparatus under drained condition. This kind of test pertains to the condition found generally in reinforced soil walls. The sample is modeled as a single element under vertical major (Σ_2) and

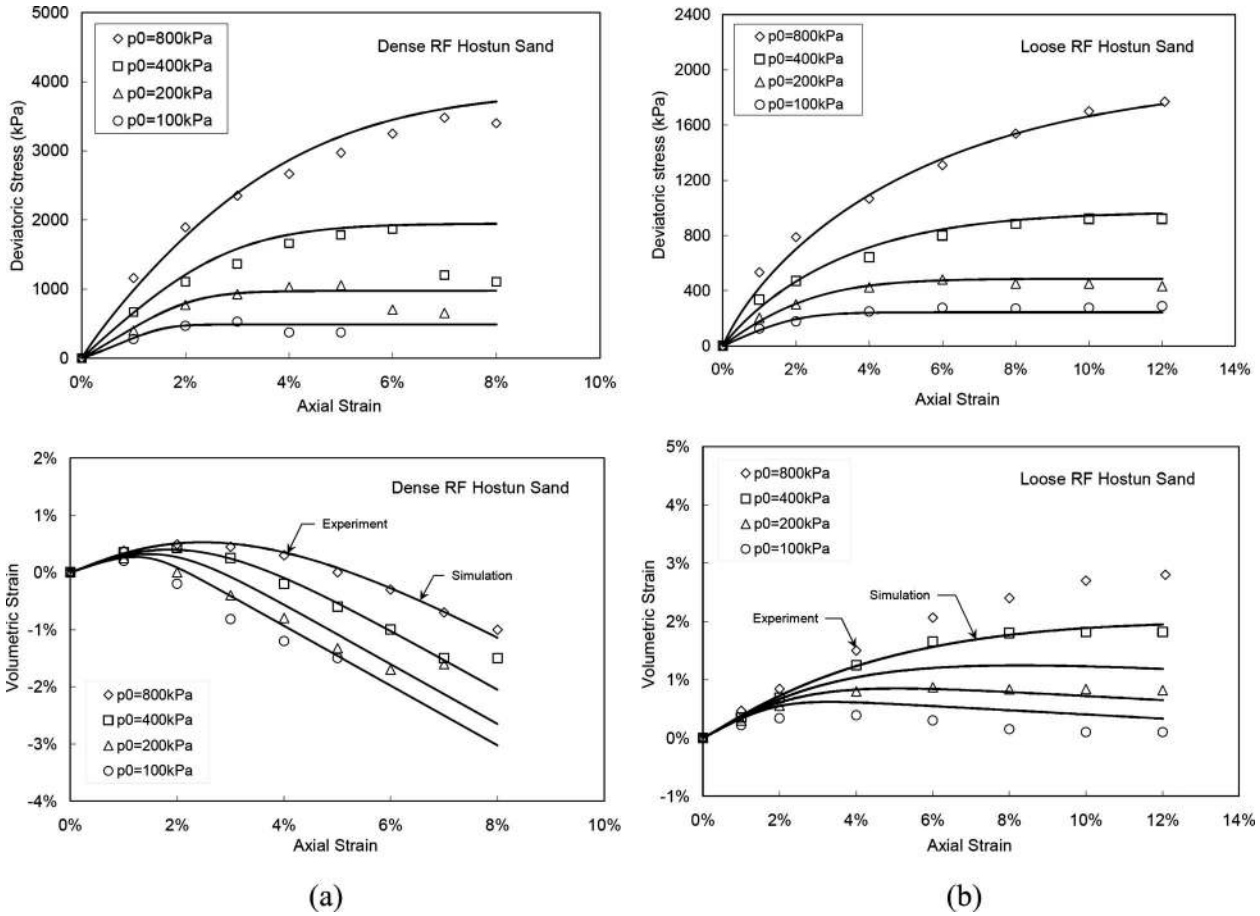

Fig. 4. Results of experimental tests from PSC tests [data from Desrues and Viggiani (2004)] and those of simulation by the proposed sand model under different lateral pressures of 100, 200, 400, and 800 kPa: (a) dense RF Hostun sand; (b) loose RF Hostun sand

Table 3. Properties of Geotextile Used in Tatsuoka and Yamauchi (1986)

Geotextile	E^{inc} (kN/m^2)	σ^{inc}_{yield} (kN/m^2)	v^{inc} (-)	Ultimate elastic strain (%)	t (mm)
Machine direction	12,000	42	0	15	4
Cross direction	5,000	18	0	15	4

constant horizontal minor (Σ_1) principal stresses. As a first step, the behavior of each constituent (soil and inclusion) is individually determined and then, based on the formulation of the two-phase system, the global behavior of such composite material is simulated. A sensitivity study on different parameters of soil and inclusion and their effect on the global behavior of reinforced soil can be found in Seyedi Hosseininia and Farzaneh (2008) in TC space. In the end, the construction behavior of a GRS wall is simulated and the results are compared with experiment.

First Series of Simulation (Tatsuoka and Yamauchi 1986)

Tatsuoka and Yamauchi (1986) performed a series PSC tests on reinforced dense Toyoura sand. The sand was reinforced by one geotextile layer, placed horizontally at the middle. The sample had the height and length of 75 and 80 mm and width of 40 mm. The sample was loaded in a strain control manner with a lateral confining pressure of Σ_1=49 kPa. The geotextile had higher stiffness in its machine direction than the cross direction. The properties are according to Table 3. In order to show the significance of the present development in the two-phase material, we first simulate the global behavior of such composite by considering the original soil model as linear elastic-perfectly plastic with Mohr-Coulomb criterion. The elastic soil parameters include Young modulus (E=12 MPa) and Poisson's ratio (v=0.4), while the plastic behavior is expressed as nonassociated with dilatancy angle ψ=9.5° and friction angle ϕ=48.3°. We have estimated the parameters according to the procedure mentioned in Brinkgreve (2005).

The results of simulation and experimental tests of unreinforced and reinforced soil samples are shown in Fig. 5(a) in terms of stress ratio (Σ_2/Σ_1) and volumetric strain along axial strain. The nonlinear growth in stress ratio of all samples is estimated by two straight lines. The first line has the same slope for all samples while the latter shows a specific slope which is related to the stiffness of inclusion. On the other hand, the results of laboratory tests show that the stress level of reinforced samples reaches a peak value in large axial strain. However, the growth in stress level in the simulations does not stop and the increase continues. This is due to the fact that no interface failure is considered in the model. Thus, the model overestimates the ultimate strength of samples reinforced by extensible inclusions. This part of behavior

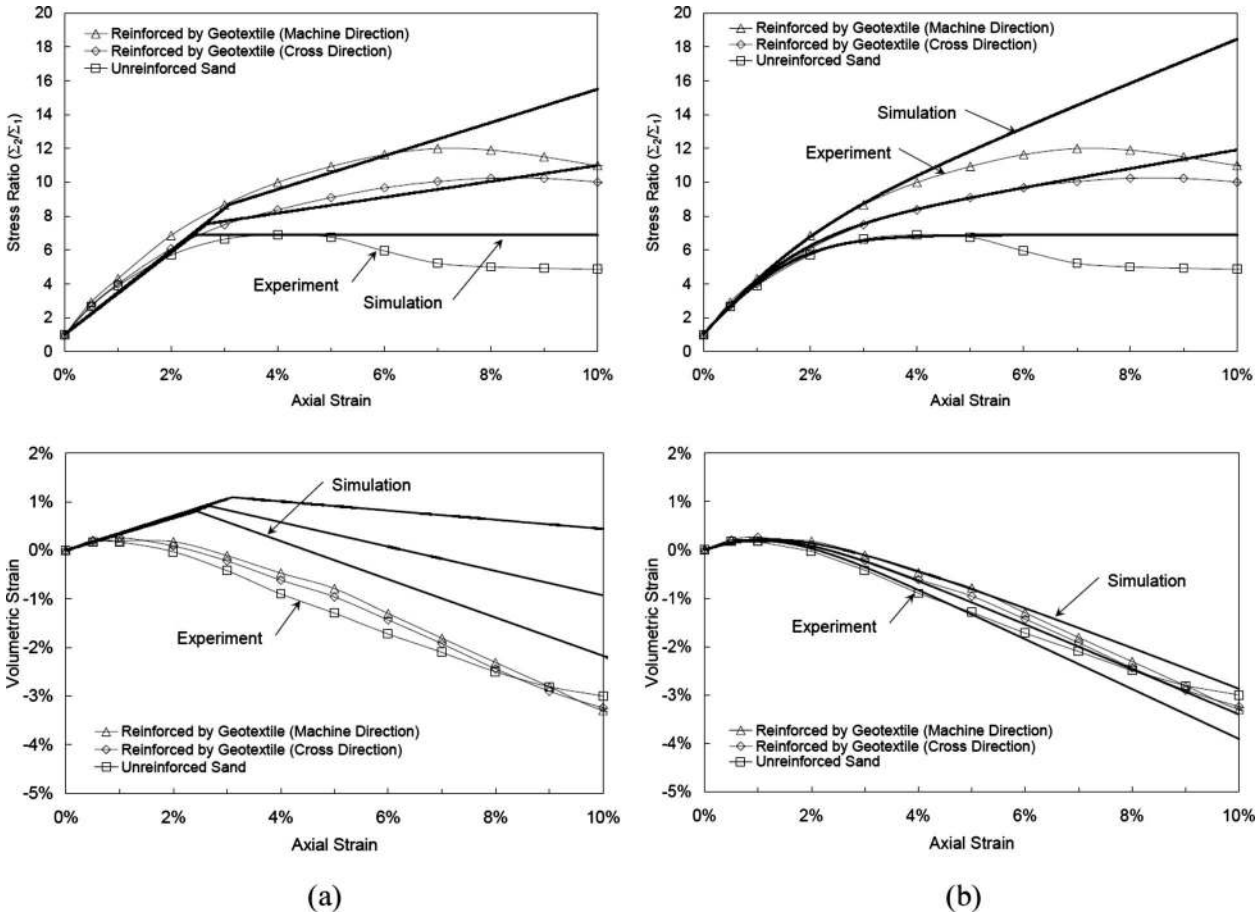

Fig. 5. Presentation of experimental and simulation results of tests on unreinforced and reinforced Toyoura sand under lateral pressure of 70 kPa [data from Tatsuoka and Yamauchi (1986)]. The inclusion is geotextile with different stiffnesses in direction. (a) Simulation by linear soil model; (b) simulation by proposed soil model.

Table 4. Model Parameters of Dense Toyoura Sand

υ (-)	G_0 (MPa)	n (-)	D_0 (-)	ϕ_{PTL} (deg)	h_0 (-)	ϕ_{peak} (deg)
0.40	8.00	0.50	0.70	27.00	0.25	48.30

at large axial strain is out of scope of the two-phase model. Referring to volumetric strain variation, it can be seen that all simulated samples show a high reduction in volumetric strain until the soil becomes plastic, where contractive behavior turns into being dilative. As can be seen, there is not a good agreement between the simulations and the experiment. In other words, the linear soil model is not liable to predict accurately the deformational regime of the samples.

Now, we simulate the behavior of Toyoura sand by the proposed model. We have calculated the parameters based on the procedure mentioned in the calibration section and they are stated in Table 4. The parameter n is assumed to be 0.5 and the G_0 is back-calculated. Fig. 5(b) presents the results of simulation and experimental behavior of unreinforced and reinforced soil samples. Despite the previous simple soil model, the results of simulation with nonlinear soil model are well fitted on the experimental results for both unreinforced and reinforced samples before the stress ratio of samples reaches the maximum value. This satisfactory agreement can be found both in stress ratio and volumetric strain. The result is less satisfactory for the machine direction, though. Referring to both experimental and simulation results, as expected, since the geotextile is stiffer in machine direction, the stress ratio grows rapidly in comparison to the sample including deformable geotextile (cross direction). Similarly, it is shown that the sample including the geotextile with stiffer direction has the least tendency in dilation among all samples.

Second Series of Simulation (Cividini 2002)

Cividini (2002) performed several PSC tests on reinforced samples with different inclusion inclinations. The cell had width and length of 40 mm and 80 mm, and height of 140 mm. The soil used was dense Ticino sand (D_r=70%). According to the procedure mentioned in the calibration section, we have obtained the soil model parameters from the test results which were performed on sand alone under different confining pressures of 50, 100, and 200 kPa. The values of parameters are listed in Table 5. Among them, the parameters n and G_0 have been derived from Fig. 6. In addition, we have simulated the soil behavior by the linear Mohr-Coulomb model with following parameters: E=30 MPa, υ=0.25, ϕ=41.8°, and ψ=19.2°. The behavior of unreinforced samples, obtained from experimental tests and simulations, is demonstrated in Fig. 7 in terms of stress difference ($\Sigma_2-\Sigma_1$) and volumetric strain versus axial strain. The comparison between experiment and simulation expresses good agreement before softening behavior by the proposed model while the linear soil model only gives us a rough estimation in trend but far from reality. The degree of discrepancy is much higher for the variation of volumetric strain. First series of reinforced samples included specimens with horizontal inclusions with the same spacing of

Table 5. Model Parameters of dense Ticino Sand (D_r=70%)

υ (-)	G_0 (MPa)	n (-)	D_0 (-)	ϕ_{PTL} (deg)	h_0 (-)	ϕ_{peak} (deg)
0.25	10.6	0.615	2.30	30.00	0.61	41.20

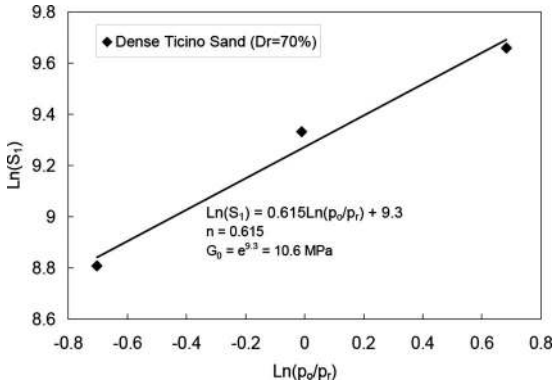

Fig. 6. Determination of elastic shear modulus parameters (G_0 and n) for dense Ticino sand

20 mm from each other. The inclusion layers used were polypropylene, nonwoven geotextile P-TS10. The properties are reported in Table 6. The samples were conducted under the same confining pressures as the unreinforced ones. The results of stress difference (Σ_2-Σ_1) versus axial strain from experimental as well as simulation tests are illustrated in Fig. 8. The variation of volumetric strain of samples is not shown here since local values of strains were measured in laboratory during the tests which seems not to be representative of the characteristics of the whole sample. Referring to Figs. 8(a and b), the simulated behavior of samples with linear and nonlinear soil models shows almost the same trend of growth in stress level as the experiment. However, it is possible to distinguish different initial slopes of curves with the nonlinear soil model while the simulation with linear soil model indicates the same slope for all samples. It is again reminded that the present model cannot predict the peak value of the composite with such extensible inclusions since no failure is considered in the contact surface (interface).

In the second part of laboratory tests, the specimens were prepared in such a way that the inclined inclusions were laid at the inclined angle of 15°, 30°, and to 45° from horizontal direction. The tests were conducted with different inclusion spacing of 20 and 30 mm under confining pressure of 100 kPa.

The preparation of reinforced samples were in such a way that, not only the inclusion layers, but also the tamped soil layers were placed in an inclined direction. In other words, the soil would be under an anisotropic stress loading regarding the bedding angle. Since we did not have the behavior of soil samples alone (and thus soil model parameters) under such bedding angles, we have used the same parameters derived from Fig. 7 in modeling the behavior of reinforced samples with inclined inclusions.

The behavior of samples for both groups (spacing=20 and 30 mm) is illustrated in Fig. 9 in terms of stress differences ($\Sigma_2-\Sigma_1$). In accordance with the simulation results in each group, although the same soil model parameters, regardless the inclination effect, have been applied for all samples, it can be found that the model can well predict the trend in stress level in different angles so that the samples have smaller tendency in shear strength growth as the inclination increases. Such consistency between results indicates that stress field in the two-phase system is assessed with acceptable precision. Moreover, it can be figured out that the reinforcement volume ratio can have influence on the composite strength, since the stress level of reinforced soil samples with spacing of 20 mm is assessed higher than the samples with spacing of 30 mm.

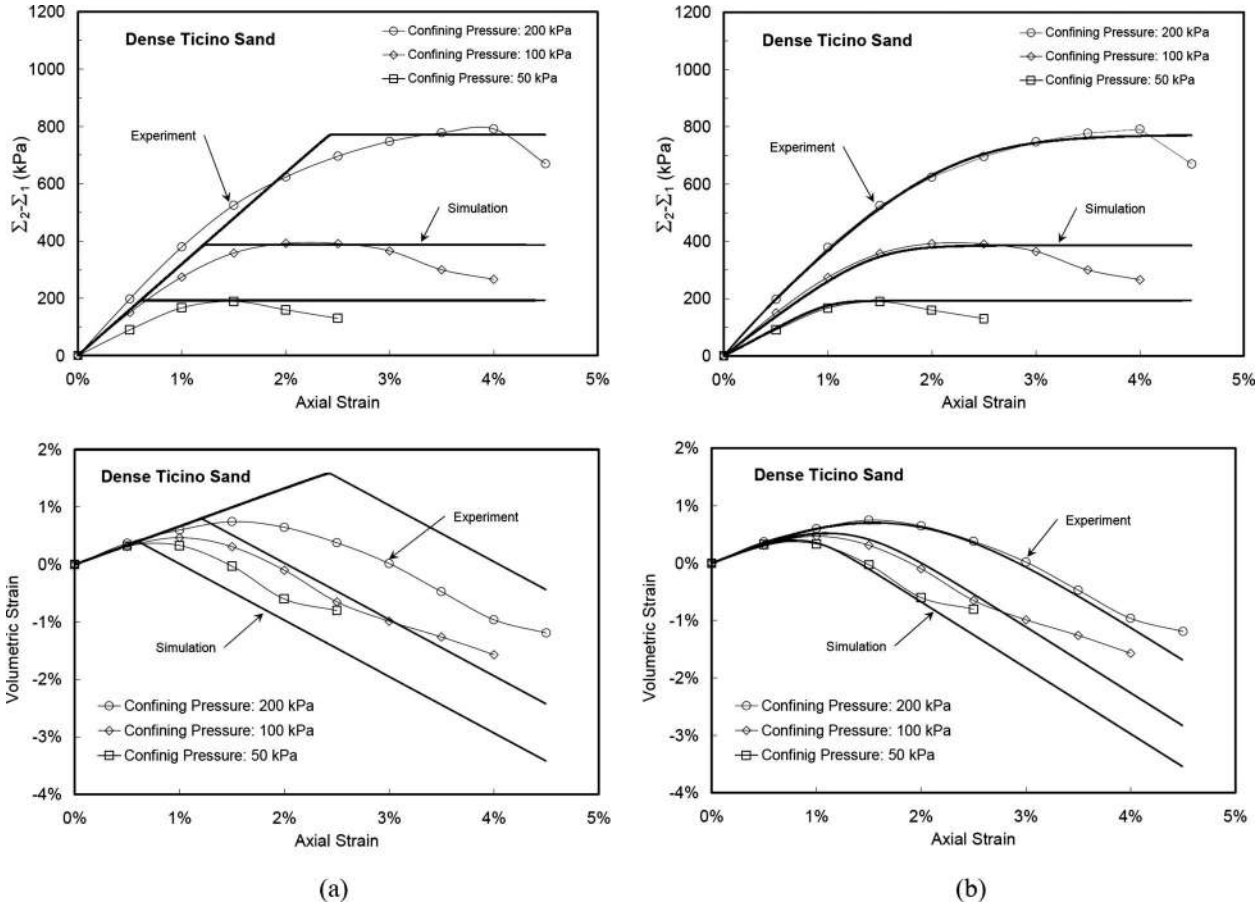

Fig. 7. Presentation of experimental and simulation results of tests on unreinforced dense Ticino sand (D_r=70%) under lateral pressure of 50, 100, and 200 kPa [data from Cividini (2002)]: (a) simulation by linear soil model; (b) simulation by the proposed soil model

Table 6. Parameters of Geotextile Used in Cividini (2002)

Geotextile	J_{ave} (kN/m)	T^{yield} (kN/m)	υ^{inc} (-)	Ultimate elastic strain (%)	t (mm)
P-TS10	11	8.8	0.1	70	1

Third Series of Simulation (McGown et al. 1978)

As the last series of single element tests, the results of several PSC tests on reinforced sand, performed by McGown et al. (1978), are referred here. The samples were tests under constant confining pressure of 70 kPa with different types of inclusion. The sand used was dense Leighton Buzzard (D_r=65%). The unit

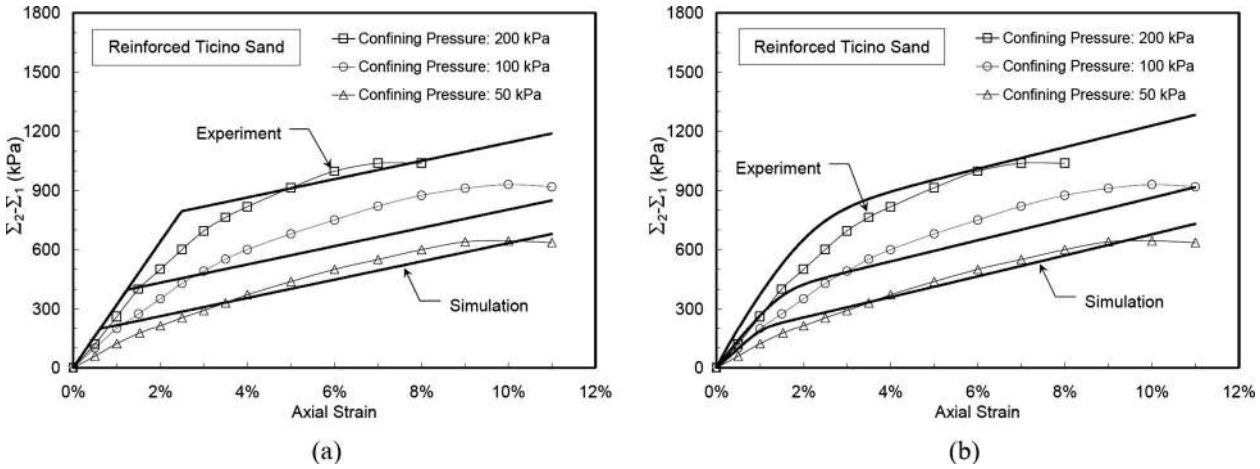

Fig. 8. Presentation of experimental and simulation results of tests on reinforced Ticino sand (D_r=70%) under lateral pressure of 50, 100, and 200 kPa [data from Cividini (2002)]: (a) simulation by linear soil model; (b) simulation by proposed soil model

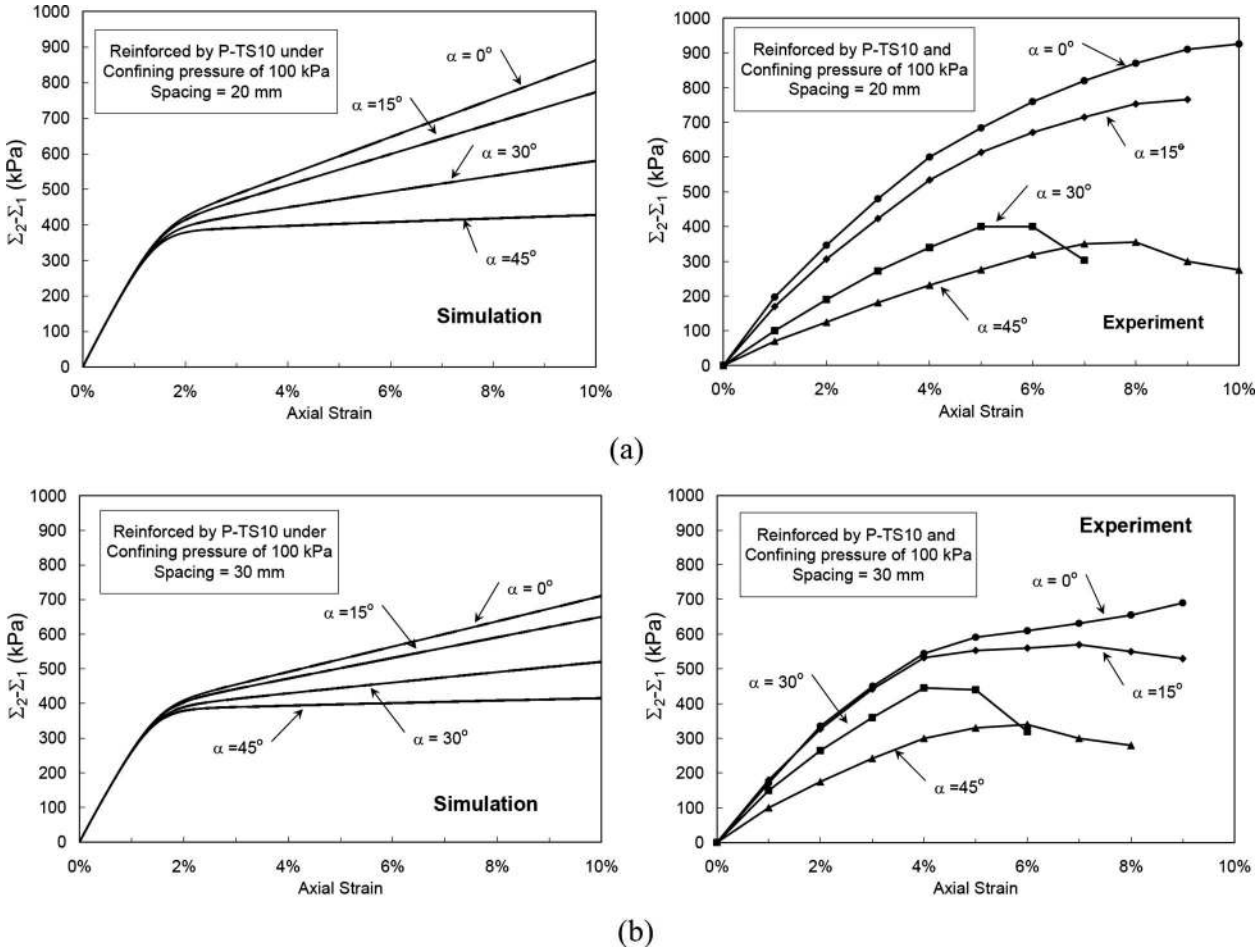

Fig. 9. Variation of stress difference for experimental and simulation tests on reinforced Ticino sand under lateral pressure of 100 kPa with different reposed angle of soil and inclusion [data from Cividini (2002)]: (a) with a spacing of 20 mm; (b) with a spacing of 30 mm

cell in the tests had the width and height of 102 mm with length of 152 mm. A horizontal inclusion layer was used to reinforce the sand.

In spite of previous series of tests where geosynthetic-type inclusions were used in the samples (high deformability), the inclusions of the present study consisted of nonwoven fabric (T140), aluminum mesh, and aluminum foil. The first type of inclusion was extensible, while the latter two ones were of inextensible type; T140 had a large deformability but the other ones had very limited range of extension. The properties of inclusions as well as soil model parameters are listed in Table 7 and 8, respectively. We have simulated the behavior of samples by considering the linear soil model too in which Young modulus is regarded as $E=52$ MPa. In the reference paper, the curve of volumetric strain versus axial strain was not reported for unreinforced sand. Thus, some assumptions for values of Poisson's ratio ($\upsilon=0.3$) and dilatancy are considered: dilatancy (D) is defined as a constant value equal to $\sin\psi$ in which $\psi=21°$.

The obtained experimental data as well as two sets of perditions of unreinforced and reinforced sand samples are shown in Fig. 10. As figured out, the simulation with linear soil model shows several breaks in the curves in addition that all samples have the same initial stiffness. However, the simulated curve of each sample with the proposed soil model is specifically distinguished by their initial slopes. For instance, the slope of sample with T140 is located between unreinforced and aluminum foil samples such as that observed in laboratory.

It is here interesting to note that the samples with aluminum foil and mesh have reached the ultimate strength in small strain level which indicates that both soil and reinforcing element have yielded as reported in laboratory too. The maximum stress ratio has been estimated with good precision too. However, such as what was observed in previous series of tests, the stress level in the sample with extensible element (T140) continues to increase

Table 7. Properties of Inclusions Used in McGown et al. (1978)

Geotextile	J_{ave} (kN/m)	T^{yield} (kN/m)	υ^{inc} (-)	Ultimate elastic strain (%)	t (mm)
Fabric (T140)	30	3.0	0	15.0	1
Aluminum mesh	200	4.0	0	2.0	1
Aluminum foil	560	1.4	0.1	0.25	1

Table 8. Model Parameters of Dense Leighton Buzzard Sand ($D_r=65\%$)

υ (-)	G_0 (MPa)	n (-)	ψ (deg)	h_0 (-)	ϕ_{peak} (deg)
0.30	62.90	0.50	21.00	0.86	51.00

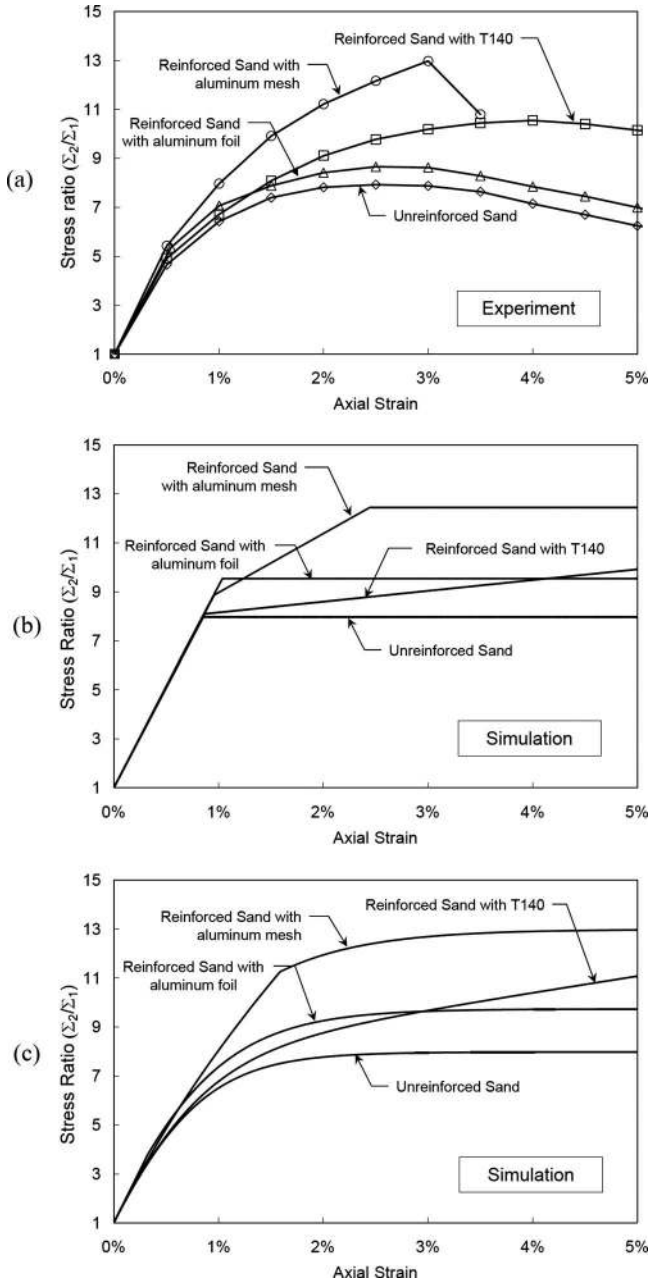

Fig. 10. Stress ratio versus axial strain diagrams for reinforced Leighton Buzzard sand samples with horizontal inclusions under lateral pressure of 70 kPa: (a) experimental data; (b) simulation by linear soil model; and (c) simulation by proposed soil model

in a gentle manner. Hence, it can be concluded that the two-phase system can predict the ultimate strength of composite only if inextensible inclusions are used in the system.

Simulation of a Full-Scale Reinforced Soil Wall

Finally, in order to demonstrate the accuracy and performance of the presented algorithm, the construction behavior of a monitored full-scale reinforced soil wall is analyzed. The wall was constructed and instrumented by the Public Works Research Institute (PWRI) in Tsukuba, Japan. Basic information of PWRI Wall has been reported by Tajiri et al. (1996). The geometry and the instrumentation of the PWRI wall is shown in Fig. 11(a). It was constructed directly on a concrete floor inside a test pit with the height of 6 m. The wall was constructed using six primary and five secondary geosynthetic layers, each 3.5 and 1.0 m long, respectively. The geosynthetic layers were bolted to the concrete modular blocks using the nuts and metal frame. The wall face consisted of a total of 12 concrete blocks with 50 cm high and 30 cm wide, except for the top and bottom blocks which were 45 and 55 cm high, respectively. The horizontal displacement of wall face was measured at 12 points along the height. Also, the strain gauges were used to measure the elongation of geogrid layers. The lateral stress behind the wall as well as vertical stress at the bottom of the wall were measured too.

The backfill used was a silty sand (D_{50}=0.42 mm, γ =16.0 kN/m^3, C_u=4.6). In order to investigate the soil behavior, three drained TC tests with confining pressures of 25, 50, and 100 kPa were applied. The proposed soil model is used to simulate the behavior and the parameters are calculated based on the calibration procedure mentioned before. The soil parameter values are depicted in Table 9. The results of experiment as well as simulations of TC tests are shown in Fig. 12 in terms of deviatoric stress and volumetric strain versus axial strain. As obvious, the model can well simulate the soil behavior obtained from triaxial tests too. For the reinforcing layers, polyethylene (HDPE) geogrid was used. The strength of the geogrid is 55 kN/m and the stiffness is taken as 800 kN/m (secant stiffness at 1.5% strain). Using large-scale direct shear tests, the interface friction angles for block-block and soil-block interactions were obtained as δ=19.6° and 16.5°, respectively.

The grid used in the numerical simulation, as shown in Fig. 11(b), consists of 589 elements. Different parts of the grid include concrete floor, concrete blocks, backfill (soil alone represented by one single phase), reinforced zones (as two-phase material) with different reinforcement volume fraction ratios, and the interface elements between dissimilar materials. The concrete floor and concrete blocks are assumed to have linear elastic behavior with the properties E=2 GPa, υ=0.17, and γ=23 kN/m^3. For interface elements, a value of 2.4×10^7 Pa/m and 10^7 Pa/m is used for normal stiffness (k_n) and shear stiffness (k_s), respectively. It is here noted that Ling et al. (2004) have analyzed the wall as a discrete model by considering separately the soil (using a generalized plasticity soil model) and reinforcement layers (using a bounding surface model). In addition, the interaction between soil and geogrid was considered by interface elements. The model was composed of 2314 elements including 115 bar elements for the inclusions. It would be of interest to say that the obtained results in the present study are very close to those of the analysis performed by Ling et al. (2004).

For brevity, the results of analysis are compared with measured data in terms of face horizontal displacement as well as strains in primary geogrids. Fig. 13 presents the wall face deformation profile in each stage of construction. As seen, there is a good agreement between the measured and analyzed results for the construction height of 4 m and above. The patterns are well replicated. It is noted that since each concrete block in the face has been represented by two nodes, the simulated results seems to be fluctuating. The strain distributions along the primary geogrid layers are depicted in Fig. 14 from both experiment and the analysis. In a general sense, it can be said that the calculated strains from the analysis have the same trend as the measured data and they match up satisfactorily to each other. According to Ling et al. (2004), the observed difference in the strain pattern could be attributed to the possible stress concentration due to uncommon connection (bolt and nut) of geogrid to blocks as well as creep in

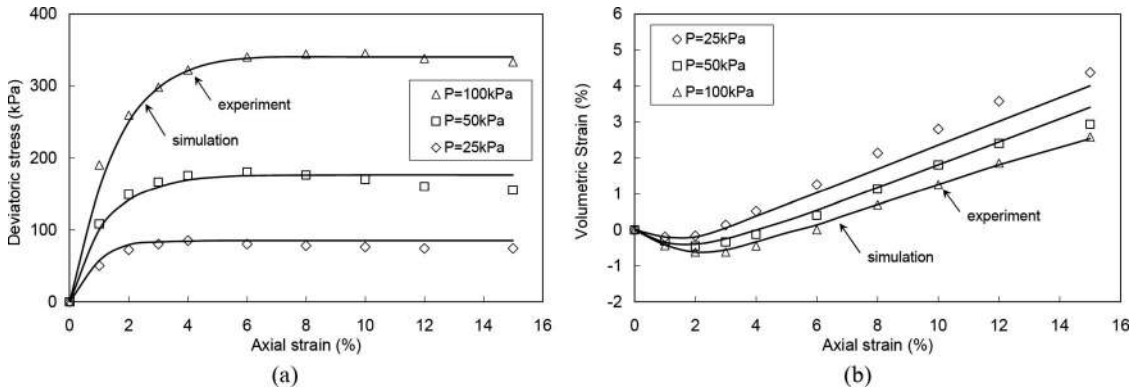

Fig. 11. Comparison between experimental and simulated soil behavior from TC tests under lateral pressure of 25, 50, and 100 kPa [data from Ling et al. (2004)]: (a) deviatoric stress versus axial strain; (b) volumetric strain versus axial strain

Table 9. Model Parameters of Silty Sand Used in PWRI Wall

v (-)	G_0 (MPa)	n (-)	D_0 (-)	ϕ_{PTL} (deg)	h_0 (-)	ϕ_{peak} (deg)
0.20	11.1	0.50	1.60	33.00	0.37	39.00

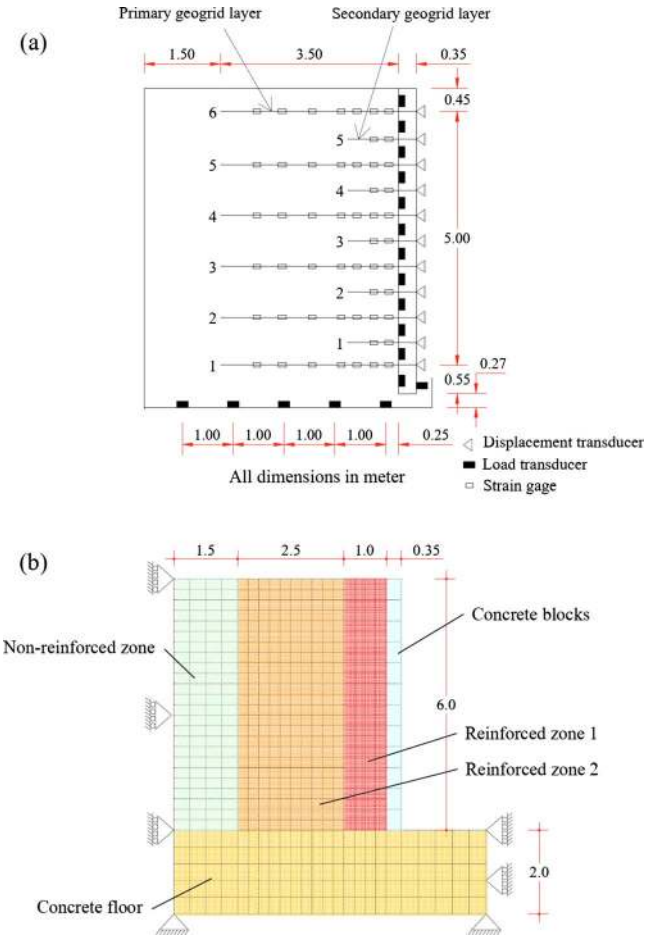

Fig. 12. PWRI wall: (a) geometry and instrumentation [after Ling et al. (2004)]; (b) grid used in numerical analysis

the geogrid that were not considered in the model. The similarity between the results of the present study with those of the analysis by Ling et al. (2004) implies that the perfect bonding hypothesis in the present analysis could have little influence on the results.

Summary and Conclusions

In the present contribution, the formulation of a two-phase system is introduced, in which a nonlinear elastoplastic constitutive model was considered for the matrix phase. The algorithm was aimed to analyze the behavior of GRS walls under operational condition rather than collapse state.

By paying attention to the soil characteristics within reinforced soil structures under working stress condition, we could introduce a relatively simple soil model. The model was defined by six parameters which can be easily obtained from conventional tests.

By implementing the proposed soil model within a two-phase system framework, it was shown that the algorithm was liable to

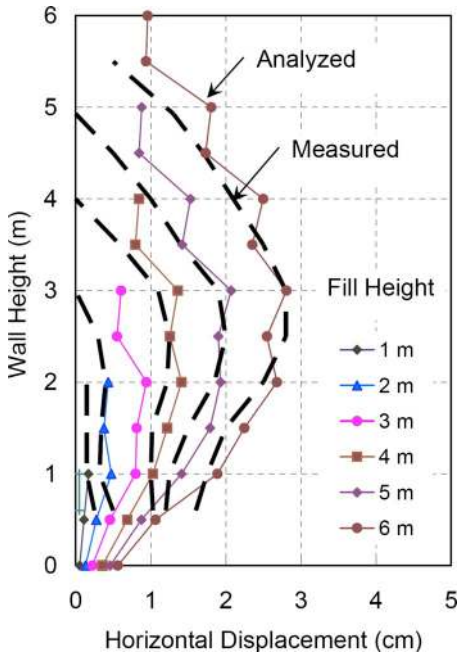

Fig. 13. Horizontal deformation of PWRI wall for different construction heights

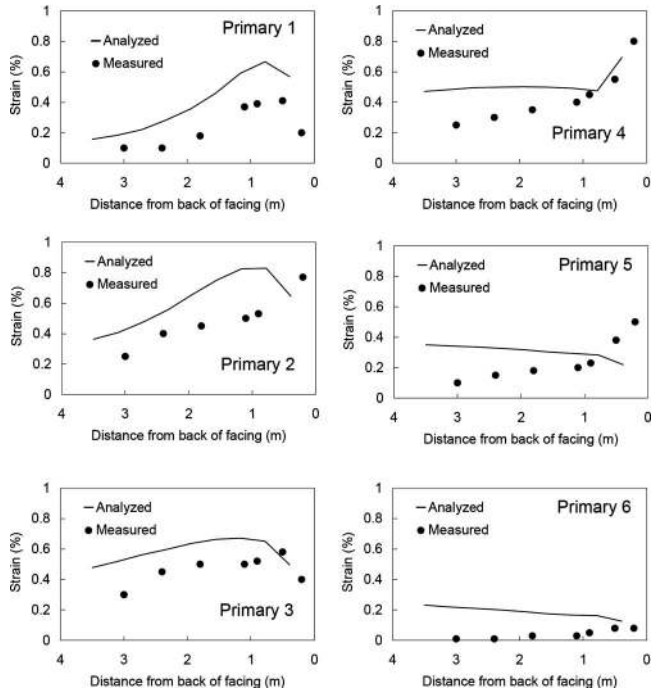

Fig. 14. Strain distribution of primary inclusions at final height (H=6 m)

predict the nonlinear prepeak behavior of single element reinforced soil samples with reasonable precision. Simulation of a full-scale reinforced soil wall indicated that the simplifications used in the soil model as well as the hypothesis of perfect bonding between phases does not considerably influence the simulation results of structures under operational conditions.

For reinforced soil systems under considerable loadings, the present algorithm should be improved. In this regard, the soil model should be able to consider post peak behavior.

Furthermore, an improvement should be accounted for interface behavior by considering relative displacement and/or contact failure between phases. The model can also be upgraded for the analysis of reinforced soil walls under cyclic loadings.

Appendix

According to Hook's law [Eq. (17)], the incremental form of elastic shear strain ($\dot{\varepsilon}_q^e$) equals

$$\dot{\varepsilon}_q^e = \dot{\varepsilon}_1^e - \dot{\varepsilon}_3^e = \frac{1}{2G}(\dot{\sigma}_1 - \dot{\sigma}_3) \tag{36}$$

Regarding the different boundary conditions in triaxial and plane strain tests, incremental volumetric strain $\dot{\varepsilon}_v^e$ is defined by

$$\dot{\varepsilon}_v^e = \dot{\varepsilon}_1^e + 2\dot{\varepsilon}_3^e = \frac{(1-2\nu)}{2G(1+\nu)}(\dot{\sigma}_1 + 2\dot{\sigma}_3) \quad \text{in triaxial test} \tag{37}$$

$$\dot{\varepsilon}_v^e = \dot{\varepsilon}_1^e + \dot{\varepsilon}_3^e = \frac{(1-2\nu)}{2G}(\dot{\sigma}_1 + 2\dot{\sigma}_3) \quad \text{in plane strain test} \tag{38}$$

Since the minor principal stress is constant in the tests, i.e., $\dot{\sigma}_3$=0, the ratio $\dot{\varepsilon}_v^e/\dot{\varepsilon}_q^e$ can be assessed accordingly as follows:

$$D_1 = \frac{\dot{\varepsilon}_v^e}{\dot{\varepsilon}_q^e} = \frac{1-2\nu}{1+\nu} \Rightarrow \nu\frac{1-D_1}{2+D_1} \quad \text{in triaxial test} \tag{39}$$

$$D_1 = \frac{\dot{\varepsilon}_v^e}{\dot{\varepsilon}^e} = 1-2\nu \Rightarrow \nu\frac{1-D_1}{2} \quad \text{in plane strain test} \tag{40}$$

References

Allen, T. M., Bathurst, R. J., Holtz, R. D., Walters, D. L., and Lee, W. F. (2003). "A new working stress method for prediction of reinforcement loads in geosynthetic walls." *Can. Geotech. J.*, 40(5), 976–994.

ASTM. (2009). "Standard test method for tensile properties of geotextiles by the wide-width strip method." *D4595-09*, Vol. 04.13, West Conshohocken, Pa.

Bathurst, R. J., Allen, T. M., and Walters, D. L. (2005). "Reinforcement loads in geosynthetic walls and the case for a new working stress design method." *Geotext. Geomembr.*, 23(4), 287–322.

Bennis, M., and de Buhan, P. (2003). "A multiphase constitutive model of reinforced soils accounting for soil-inclusion interaction behavior." *Math. Comput. Modell.*, 37, 469–475.

Brinkgreve, R. B. J. (2005). "Selection of soil models and parameters for geotechnical engineering application." *Soil constitutive models: Evaluation, selection, and calibration*, A. Yamamuro and V. N. Kaliakin, eds., ASCE, Reston, Va., 128.

Cividini, A. (2002). "A laboratory investigation on the behavior of reinforced sand samples under plane strain and triaxial conditions." *Soils Found.*, 42(6), 23–39.

Dafalias, Y. F. (1986a). "An anisotropic critical state soil plasticity model." *Mech. Res. Commun.*, 13(6), 341–347.

Dafalias, Y. F. (1986b). "Bounding surface plasticity, I: Mathematical foundation and hypoplasticity." *J. Eng. Mech.*, 112(12), 1263–1291.

Dafalias, Y. F., and Popov, E. P. (1975). "A model of nonlinearly hardening materials for complex loading." *Acta Mech.*, 21, 173–192.

de Buhan, P., Bourgeois, E., and Hassen, G. (2008). "Numerical simulation of bolt-supported tunnels by means of a multiphase model conceived as an improved homogenization procedure." *Int. J. Numer. Analyt. Meth. Geomech.*, 32(13), 1597–1615.

de Buhan, P., Mangiavacchi, R., Nova, R., Pellegrini, G., and Salencon, J. (1989). "Yield design of reinforced earth walls by a homogenization method." *Geotechnique*, 39, 189–201.

de Buhan, P., and Sudret, B. (1999). "A two-phase elastoplastic model for unidirectionally-reinforced materials." *Eur. J. Mech. A/Solids*, 18, 995–1012.

de Buhan, P., and Sudret, B. (2000). "Micropolar multiphase model for materials reinforced by linear inclusions." *Eur. J. Mech. A/Solids*, 19, 669–687.

Desai, C. S., and El-Hoseiny, K. H. (2005). "Prediction of field behavior of reinforced soil wall using advance constitutive model." *J. Geotech. Geoenviron. Eng.*, 131(6), 729–739.

Desrues, J., and Viggiani, G. (2004). "Strain localization in sand: An overview of the experimental results obtained in Grenoble using stereophotogrammetry." *Int. J. Numer. Analyt. Meth. Geomech.*, 28, 279–321.

Duncan, J. M., and Chang, C. Y. (1970). "Nonlinear analysis of stress and strain in soils." *J. Soil Mech. Found. Div.*, 99(SM5), 1629–1653.

Guler, E., Hamderi, M., and Demirkan, M. M. (2007). "Numerical analysis of reinforced soil retaining wall structures with cohesive and granular backfills." *Geosynthet. Int.*, 14(6), 330–345.

Harrison, W.J., and Gerrard, C. M. (1972). "Elastic theory applied to reinforced earth." *J. Soil Mech. And Found. Div.*, 98(12), 1325–1345.

Hassen, G., and de Buhan, P. (2005). "A two-phase model and related numerical tool for the design of soil structures reinforced by stiff linear inclusions." *Eur. J. Mech. A/Solids*, 24, 987–1001.

Hatami, K., and Bathurst, R. J. (2005). "Development and verification of

a numerical model for the analysis of geosynthetic reinforced soil segmental walls under working stress conditions." *Can. Geotech. J.*, 42(4), 1066–1085.
Hatami, K., and Bathurst, R. J. (2006). "A numerical model for reinforced soil segmental walls under surcharge loading." *J. Geotech. Geoenviron. Eng.*, 132(6), 673–684.
Helwany, S. M. B., Reardon, G., and Wu, J. T. H. (1999). "Effects of backfill on the performance of GRS retaining walls." *Geotext. Geomembr.*, 17(1), 1–16.
Holtz, R. D., and Lee, W. F. (2002). "Internal stability analysis of geosynthetic reinforced retaining walls." *Technical Rep. Prepared for Washington State Transportation Commission*.
Ishihara, K. (1996). *Soil behavior in earthquake geotechnics*, Clarendon, Oxford, U.K.
Karpurapu, R., and Bathurst, R. J. (1995). "Behavior of geosynthetics reinforced soil retaining walls using the finite-element method." *Comput. Geotech.*, 17(3), 279–299.
Krieg, R. D. (1975). "A practical two-surface plasticity theory." *ASME J. Appl. Mech.*, 42, 641–646.
Lade, P. V., and Duncan, J. M. (1973). "Cubical triaxial tests on cohesionless soil." *J. Soil Mech. and Found. Div.*, 99(SM10), 793–812.
Leshchinsky, D., and Vulova, C. (2001). "Numerical investigation of the effects of geosynthetic spacing on failure mechanisms in MSE block walls." *Geosynthet. Int.*, 8(4), 343–365.
Li, X. S. (2002). "A sand model with state-dependent dilatancy." *Geotechnique*, 52(3), 173–186.
Li, X. S., and Dafalias, Y. F. (2000). "Dilatancy for cohesionless soils." *Geotechnique*, 50(4), 449–460.
Ling, H. I., Cardany, C. P., Sun, L.-X., and Hashimoto, H. (2000). "Finite-element study of a geosynthetic-reinforced soil retaining wall with concrete-block facing." *Geosynthet. Int.*, 7(3), 163–188.
Ling, H. I., and Leshchinsky, D. (2003). "Finite-element parameter studies of the behavior of segmental block reinforced soil retaining walls." *Geosynthet. Int.*, 10(3), 77–94.
Ling, H. I., and Yang, S. (2006). "A unified sand model based on critical state and generalized plasticity." *J. Eng. Mech.*, 132(12), 1380–1391.
Ling, H. L., Liu, H., Kaliakin, V. N., and Leshchinsky, D. (2004). "Analyzing dynamic behavior of geosynthetic-reinforced soil retaining walls." *J. Eng. Mech.*, 130(8), 911–920.
Manzari, M. T. (1994). "Finite deformation analysis and constitutive modeling of a non-cohesive soils for liquefaction problems." Ph.D. dissertation, Univ. of California, Davis, Calif.
McGown, A., Andrawes, K. Z., and Hasani, M. M. (1978). "Effect of inclusion properties on the behavior of sands." *Geotechnique*, 28(3), 327–346.
Michalowski, R. L., and Zhao, A. (1995). "Continuum versus structural approach to stability of reinforced soil." *J. Geotech. Eng.*, 121, 152–162.
Mroz, Z., and Zienkiewicz, O. C. (1984). "Uniform formulation of constitutive equations for clays and sand." *Mechanics of engineering materials*, C. S. Desai and R. H. Gallagher, eds., Chapter 22, Wiley, New York, 415–459.
Nova, R., and Wood, D. M. (1979). "A constitutive model for sands in triaxial compression." *Int. J. Numer. Analyt. Meth. Geomech.*, 3, 255–278.
Pastor, M., Zienkiewicz, O. C., and Chan, A. H. C. (1990). "General plasticity and the modelling of soil behavior." *Int. J. Numer. Analyt. Meth. Geomech.*, 14, 151–190.
Romstad, K.M., Herrmann, L.R., Shen, C.K. (1976). "Integrated study of reinforced earth—I: Theoretical formulation." *J. Geotech. Engrg. Div.*, 102(GT5), 457–471.
Seyedi Hosseininia, E. (2008). "A contribution to development of multiphase model by considering the non-linear behavior of matrix applied to geosynthetics-reinforced soil (GRS) structures." Ph.D. dissertation, Univ. of Tehran, Iran (in Persian).
Seyedi Hosseininia, E., and Farzaneh, O. (2008). "Presentation of a homogenized multi-phase model for reinforced soil considering nonlinear behavior of matrix." *Proc., 12th Int. Conf. Int. Assoc. for Comp. Meth. and Adv. in Geomech. (IACMAG)*, Goa, India.
Sudret, B. (1999). "Modélisation multiphasique des ouvrages renforcés par inclusions." Ph.D. thesis, Ecole nationale des ponts et chaussées, Paris (in French).
Sudret, B., and de Buhan, P. (2001). "Multiphase model for inclusion-reinforced geostructure: Application to rock-bolted tunnels and piles raft foundations." *Int. J. Analyt. Meth. Geomech.*, 25, 155–182.
Tatsuoka, F., and Yamauchi, H. (1986). "A reinforcing method for steep clay slopes with non-woven fabric." *Geotext. Geomembr.*, 4(3–4), 241–268.
Thai, S. Q., Hassen, G., and de Buhan, P. (2009). "A multiphase approach to the stability analysis of reinforced earth structures accounting for a soil-strip failure condition." *Comput. Geotech.*, 36, 454–462.
Wang, Z., Dafalias, Y. F., and Shen, C. (1990). "Bounding surface hypoplasticity model." *J. Eng. Mech.*, 116(5), 983–1001.
Yang, B. L., Dafalias, Y. F., and Herrmann, L. R. (1985). "A bounding surface plasticity model for concrete." *J. Eng. Mech.*, 111(3), 359–380.